Numerical and Experimental Study of Acoustic Emission Source Signal Reconstruction in Fibre-Reinforced Composite Panels

Huijer, A.J.; Kassapoglou, Christos; Pahlavan, Lotfollah

Important note
To cite this publication, please use the final published version (if applicable).
Please check the document version above.

Numerical and Experimental Study of Acoustic Emission Source Signal Reconstruction in Fibre-Reinforced Composite Panels

Arnaud Huijer[1]([✉]), Christos Kassapoglou[2], and Lotfollah Pahlavan[1]

[1] Faculty of Mechanical, Maritime and Materials Engineering,
Delft University of Technology, Mekelweg 2, Delft, The Netherlands
`a.j.huijer@tudelft.nl`
[2] Faculty of Aerospace Engineering, Delft University of Technology,
Kluyverweg 1, Delft, The Netherlands

Abstract. The recording and processing of acoustic emissions can be used to identify and localise damage mechanisms occurring in engineering structures. In plate-like structures, acoustic emissions propagate through the structure as guided waves. With a measurement location away from the source location, dispersion effects in the guided wave distort the acoustic emission signal. The distortion of the original signal hampers identification of damage mechanisms.

This research describes and assesses a method to reconstruct the original acoustic emission signal using dispersion compensation. Simulations and experiments are performed involving thick glass-fibre reinforced plastic laminates. The signal reconstruction on the simulated data gives a reasonable representation of the simulated signal at the location of interest. In the experimental case, similarity slightly degrades. Deviation in arrival time between original measurement and reconstruction is attributed to a possible discrepancy in material properties in reality versus the properties used in the reconstruction.

Keywords: Dispersion compensation · Acoustic emission · Damage identification · Fibre-reinforced plastics · Guided waves

1 Introduction

In engineering materials the onset and growth of defects is typically accompanied by sudden releases of energy, which are called acoustic emissions (AE). It has been shown that specific damage mechanisms have distinct AE signatures [1]. This enables possibility of identification of damage mechanisms on the basis of AE measurements.

In plate-like structures, the AE signals can propagate as guided waves. The velocity and attenuation behaviour in guided waves is dependent on material and geometrical properties and on the frequency content of the AE. In the case of anisotropic plates, it is further dependent on the direction of propagation of the guided wave [2, 3]. This behaviour implies that measurement of a single AE will be different at different measurement locations. As such, for reliable identification of damage mechanisms through AE evaluation, differences in measurement due to wave propagation effects need to be accounted for.

Wave propagation effects can be accounted for by reconstructing source AE signals at the source location from the measurement signals. Several methods exist that allow signal reconstruction including dispersion compensation. Among them are Time Reversal (TR) and Fourier-domain dispersion compensation [4].

In active TR, the guided wave generated by transducer A is measured by transducers B, reversed in time, re-emitted from B and measured by A. In passive TR, the re-emission from B takes place in a simulation [5]. For AE signal reconstruction of pencil lead breaks and broadband signals, Falcetelli et al. [6, 7] provided transfer functions in isotropic thin panels using active TR. In thin fibre-reinforced plastic (FRP) panels, signal reconstruction was performed by means of active [8] and passive [5] TR.

Fourier-domain dispersion compensation has conceptual similarities with passive TR [9, 10]. The method typically makes use of a priori known wavenumber-frequency dispersion relations to analytically reconstruct a source waveform. Different approaches exist [4, 11]. Fourier-domain signal processing has been applied in the active localisation of damage and phase reconstruction in isotropic materials [9, 12, 13] and FRPs [4, 14].

This paper assesses the accuracy of a dispersion compensation technique, based on Fourier-domain signal processing, towards the reconstruction of AE waveforms in FRP materials. The accuracy will be evaluated by comparison between measurements at a specific location and reconstructions from other measurements towards this location. By considering both measurements from numerical simulations through 3D transient Spectral Element Model (SEM) and experimental measurements, the error originating from the reconstruction method can be distinguished from the error due to uncertainties in the experimental setup and the assumed material properties.

Firstly the mathematical procedure is explained, including the approach to dispersion compensation and the method for obtaining dispersion curves from known material properties. Secondly, details on acquiring simulated measurement data from 3D SEM are explained. This is followed by explanation of the experimental procedure. Subsequently, results from the measurements and assessment of the reconstruction accuracy are presented. Lastly, conclusions are presented and an outlook on further work is shared.

2 Mathematical Procedure

2.1 Dispersion Compensation

Three topics may be discerned when reconstructing a source signal through dispersion compensation of measurement signals. Firstly the trajectory from source to receiver needs to be determined. Secondly, for this trajectory, dispersion curves are attained. Thirdly, with these dispersion curves, dispersion compensation on the measurement signals can be performed. The process is visualised in Fig. 1.
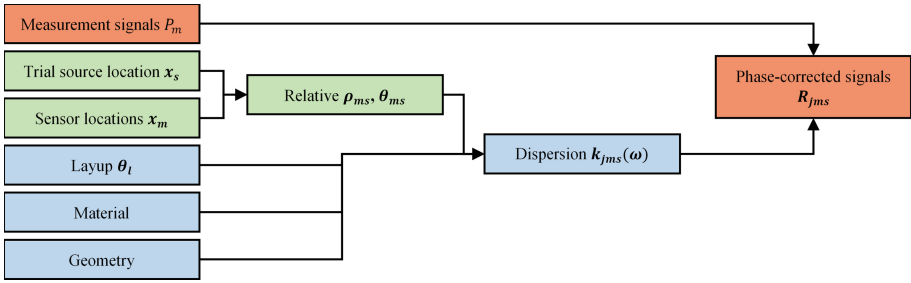
Fig. 1. Process of dispersion compensation in anisotropic materials.

From an anticipated source location s and known measurement locations m, relative propagation directions θ_{ms} and distances ρ_{ms} are determined. Given material properties, plate thickness and FRP stacking sequence θ_l relative to the propagation direction θ_{ms}, the dispersion curves can be constructed.

Dispersion curves are obtained using a semi-analytical formulation as described by Wang and Yuan [15] and Pahlavan [5]. In this formulation the displacement field over the plate thickness undergoes a series expansion up to the third order. Applying Hamilton's principle and adequate stress-strain relations, the equation of motion is acquired. In the absence of external loads and considering harmonic motion, this is simplified to a polynomial Eigenvalue problem. Eigenvalues contain wavenumbers $k_{jms}(\omega)$ for the symmetric, antisymmetric and shear horizontal modes j as function of circular frequency ω.

To allow for dispersion compensation, measurement signals $P_m(t)$ in time t are described in the frequency domain $\widehat{P}(\omega)$. For every frequency, a phase correction is applied given the corresponding distances ρ_{ms} and wavenumbers $k_{jms}(\omega)$. The resulting corrected signal $\hat{R}_{jms}(\omega)$ is shown in Eq. (1).

$$\widehat{R}_{jms}(\omega) = \widehat{P}_m(\omega)e^{-ik_{jms}(\omega)\rho_{ms}} \tag{1}$$

Back in the time domain, dispersion corrected signals $R_{jms}(t)$ are obtained (Eq. (2)).

$$R_{jms}(t) = \frac{1}{2\pi}\int_{-\infty}^{\infty}\widehat{R}_{jms}(\omega)e^{i\omega t}d\omega \tag{2}$$

2.2   Waveform Similarity

To evaluate the accuracy of the reconstruction, a comparison is made between reconstructions $R_{jmr}(t)$ towards location r close to the emission source and the direct measurement at that location $P_r(t)$. It is recognised that in direct reconstruction, a discrepancy in trajectory from measurement m to source s and to reference r would exist. This is addressed by performing a reconstruction towards s and using the same method to perform a forward reconstruction from s to r. This is shown in Eq. (3) and in Fig. 2.
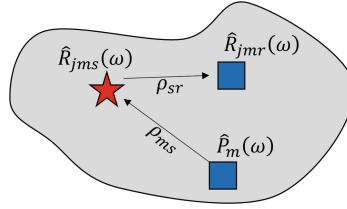
Fig. 2. Illustration of the reconstruction procedure from measurement to source to reference measurement.

$$\widehat{R}_{jmr}(\omega) = \widehat{R}_s(\omega)e^{iK_{jrs}(\omega)\rho_{rs}} \qquad (3)$$

Comparison between $R_{jmr}(t)$ and $P_r(t)$ is done via waveform similarity. Note that in the method of Eq. 1, no correction for attenuation is considered. A normalised waveform similarity as described in Eq. (4) is used for each single reconstructed signal $R_{jmr}(t)$.

$$Similarity_{jmr} = \max\left(\frac{(R_{jmr}(t)\star P_m(t))(\tau)}{\sqrt{(R_{jmr}(t)\star R_{jmr}(t))(\tau_0)(P_m(t)\star P_m(t))(\tau_0)}}\right) \qquad (4)$$

The five-pointed star $\star$ indicates cross-correlation and τ indicates lag (with $\tau_0 = 0$). Time delay is defined as the argument of the maximum similarity value. This is then divided by the period related to the centre frequency of the input signal to get a normalised time delay. Note that the similarity values are relevant for waveform clustering, while time delay is an indication of localisation error.

3 Simulation Using 3D SEM

In order to assess the reconstruction method without experiment-related biases, a simulated measurement dataset was generated. The simulation came in the form of a transient linear elastic spectral element analysis (SEM). SEM is frequently used in time domain guided wave simulations [16]. In SEM, field variables are approximated using higher-order polynomial basis functions. These basis functions allow for a higher convergence rate compared to traditional finite element methods [17]. In the case of Legendre-Gauss-Lobatto-Lagrange polynomials the mass matrix becomes diagonal, reducing the number of operations in the time integration process [5, 17].

The simulation was performed on a model that has close similarities to the experiment described in the following section. The domain considered in the simulation is a GFRP laminate with the properties given in Table 1. The domain had length, width and thickness dimensions of 600 mm, 600 mm and 10.2 mm. The domain consisted of 900 elements with 20 mm length and width and fourth-order polynomials. In the thickness direction, the elements had a size of 10.2 mm and were of fourth-order as well. These values are based on a mesh convergence study. A 1 N amplitude five-cycle Hanning-windowed

pulse with a centre frequency of 40 kHz was excited at a location 250 mm away from the edges of the domain. The excitation was given in the out-of-plane direction. The propagated wave was measured on a grid of 100×100 mm, with a spacing of 20 mm. In Fig. 3, the domain and a snapshot of the propagating wave can be seen.

Table 1. Lamina material properties used in the 3D SEM simulation and for reconstruction of the experimental data.

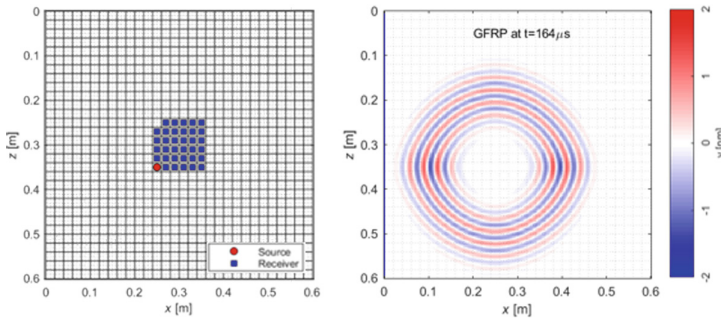| E_1 (GPa)	$E_2 = E_3$ (GPa)	$G_{12} = G_{13}$ (GPa)	G_{23} (GPa)	$\nu_{12} = \nu_{13}$ (GPa)	ν_{23} (GPa)	ρ (kg/m^3)
46.2	13.1	4.1	5.1	0.29	0.28	1872

Fig. 3. Discretisation of a GFRP plate. The left figure shows the domain, with mesh and integration points given in black lines and dots. The right figure shows the vertical motion of the simulated unidirectional GFRP plate that has been excited in the out-of-plane direction with a five cycle burst with 40 kHz centre frequency.

4   Experimental Procedure

To test the method in a more realistic environment, experiments have been performed in a manner similar to the simulation. In this situation, the reconstruction is additionally subject to discrepancies such as variation in material properties over location and damping effects. The experiment as such can be seen as a measure of robustness in a reasonably realistic context.

The setup is shown in Fig. 4 and follows the subsequent order: an actuator (denoted by 'a' and of the type VS600-Z1) emits an artificial signal that is generated by an arbitrary waveform generator (1, Siglent SDG10251) and that is amplified (2, Falco WMA-300) with 34 dB. This signal propagates as a guided wave through a thick GFRP panel (3) and is measured by both a reference sensor (b) and a measurement sensor (c). Both measurements are amplified (5, Vallen AEP5H) with 40 dB and recorded by a data acquisition system (6, Vallen AMSY-6). The signals are then stored on a measurement laptop (7).

The GFRP panel is made from E-glass fibres with a vinyl ester resin. The laminate layup is [05,905]s and has a total thickness of 10.2 mm [18]. Material properties that are used for reconstruction are stated in Table 1. The resin infusion manufacturing process allows for slight global or local variations in material properties.

The actuator and reference sensor (a & b) are coupled to the panel by means of hot-melt adhesive. This ensures that the transmission of the emitted signal is not altered over time. Measurement sensor (c) is positioned and repositioned on a grid of 100 mm × 100 mm, with a spacing of 20 mm. Using the same sensor for each location prevents variation in measurements due to variation in sensor properties. As a coupling agent, medical ultrasonic gel is applied between the test panel and the measurement sensor. Constant pressure on the measurement sensor is provided by a weight (4).
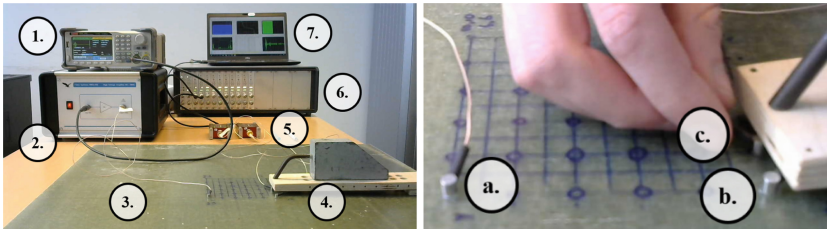

Fig. 4. Experimental setup: The left figure shows a general overview and the right figure is a close-up. Numbers 1–7 relate to the Siglent SDG10251 waveform generator, Falco WMA-300 amplifier, test specimen, measurement sensor fixture, Vallen AEP5H preamplifiers, Vallen AMSY-6 data acquisition system and measurement laptop, respectively. Letters a-c denote the actuator, reference sensor and measurement sensor. All transducers are of the VS600-Z1 type.

The source signal S emitted by the waveform generator is a five-cycle Hanning-windowed sine wave with a centroid frequency of 40 kHz. The signal is shown in Fig. 5 in time and frequency domains. The limited amount of cycles and associated short duration of the signal allows for measurements to be minimally influenced by interference patterns. Further, a band of frequencies is excited that will introduce dispersive effects in the measurements. As the measurement sensor is repositioned during the experiments, the source signal is emitted repeatedly.
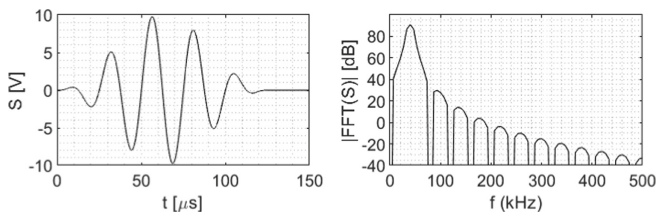

Fig. 5. Source signal S in time domain (left figure) and frequency domain (right figure).

The measurement by the reference and measurement sensors is based on full-waveform capture. The signals were recorded using hit definition, keeping a 50 dB threshold. Sampling frequency for the waveform was 5 MHz. A digital band-pass filter was applied, ranging from 25 kHz to 850 kHz. Total duration of the recording of the waveform was 1638.4 µs, including 200 µs pretrigger time. Rearm time (hit lockout time) and duration discrimination time (hit definition time) were chosen to be 250 µs.

5   Numerical and Experimental Results and Analysis

5.1   Simulation Results of GFRP Panel

Based on the simulation and mathematical procedure described above, similarity is assessed between the measurements at location (20,80)mm close to the source and reconstructions based on measurements at the other locations. In the simulation, the prescribed motion was in out-of-plane direction. Based on this, the reconstruction procedure adopted a dispersion curve related to the antisymmetric wavemode. In Fig. 6, the similarity index described in Eq. (4) is shown on the left. The normalised time lag is given on the right. In Fig. 7, a comparison over time is made between the measurement at (20,80)mm and reconstructions at selected other locations.
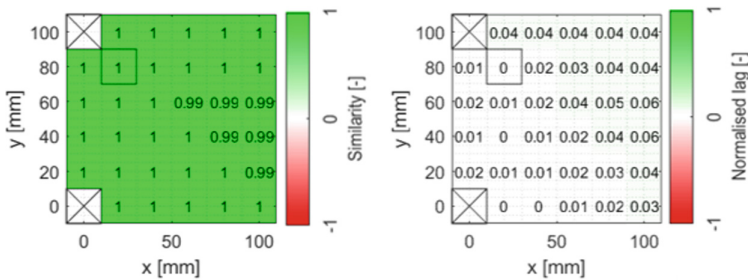

Fig. 6. Comparison between simulated response in out-of-plane direction v[nm] at location (20,80)mm and reconstructions from measurements at other locations towards this location. The left figure shows the Similarity index between the measurement and the reconstructions. The right figure shows the lag relative to a period in the signal (1/(40 kHz)).
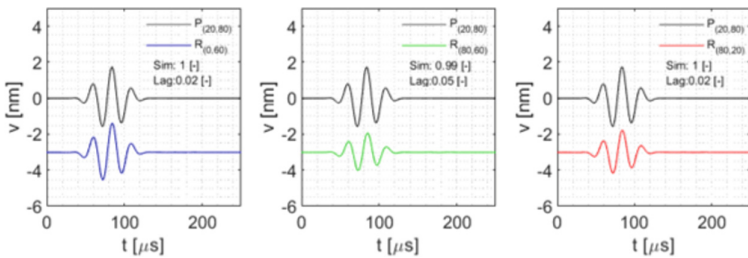

Fig. 7. Three graphs with comparison between a measurement P and individual reconstruction R. The similarity index is denoted by 'Sim' and the normalised lag by 'Lag'.

The figures present that the original measurement and reconstructions are near identical in shape and time delay. The minor deviations are considered to be coming from contributions from other wavemodes or from effects related to differences between SEM through-thickness discretisation and the semi-analytical reconstruction. In general, the results demonstrate that the reconstruction procedure can give viable outcomes.

5.2   Experiment on GFRP Panel

The experiment described in the section above makes use of the repositioning of the measurement sensor. Actuation therefore is repeated over time. Similarity-based time picking on the measurements of the reference sensor has been used to correct for the different location of the measurement sensor. This ascertains that the measurements are assessed with a correct time delay with respect to the source. In Fig. 8, corrected measurements are shown for four emission repetitions per sensor position.
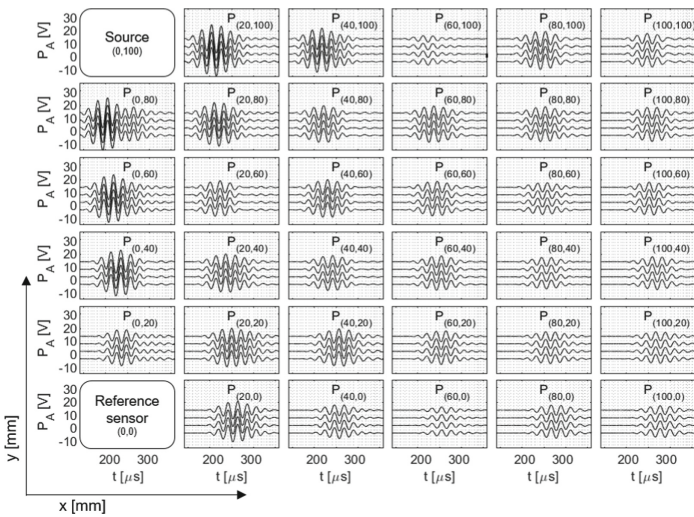

Fig. 8. Waveforms $P_{(i,j)}$ in voltage over time measured by the sensor at location $(x,y) = (i,j)$ from the reference. Note the monotonic delay in time away from the source and the phase of the signal varying over location.

The graphs show that the measurements are repeatable and that the time delay is consistent. In the experiment, the excitation was applied only on the top face of the panel. For that reason, antisymmetric wave motion is considered in the reconstruction. Similar to the assessment of the simulated data, comparison is made between the measurement at location (20,80)mm and reconstructions from other locations towards this location. The comparison is visualised in Fig. 9 and Fig. 10.
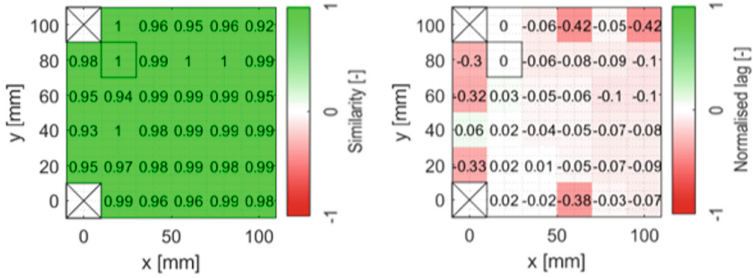
Fig. 9. Comparison between experimental measurement in voltage amplitude P_A [V] at location (20,80)mm and reconstructions from measurements at other locations towards this location. The left figure shows the Similarity index between the measurement and the reconstructions. The right figure shows the lag relative to a period in the signal (1/(40 kHz)).
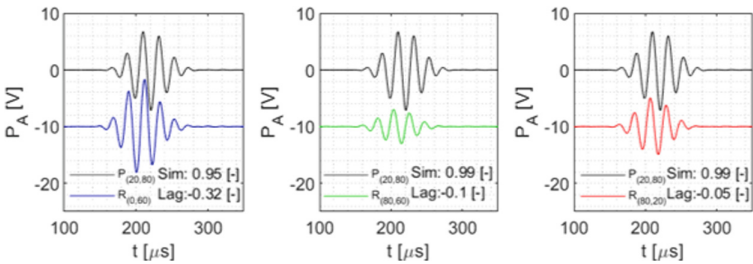

Fig. 10. Three graphs with comparison between a measurement P and individual reconstruction R. The similarity index is denoted by 'Sim' and the normalised lag by 'Lag'.

From the results it appears that the reconstruction has slightly lower similarity values compared to the results from the simulation. Further, the normalised lags show deviation in time delay between the reconstructions and the measurement. It is expected that a discrepancy in material properties is the main cause.

6   Conclusion

This research assessed the accuracy of signal reconstruction using dispersion compensation based on semi-analytical dispersion curves. Simulations and experiments are performed involving thick GFRP laminates. The signal reconstruction on the simulated data, considering a narrow-band pulse, is reasonably similar to the simulated measurement. In the experimental case, similarity slightly drops. Deviation in arrival time between original measurement and reconstruction is attributed to a discrepancy in material properties in reality versus the properties used in the reconstruction.

Recommendations include assessment of the influence of deviation in the material properties on the arrival time accuracy. Further evaluation using signals closer to actual acoustic emission events is considered. In a later stage, the method will be extended from plates to more complex geometries.

References

1. Saeedifar, M., Zarouchas, D.: Damage characterization of laminated composites using acoustic emission: a review. Compos. Part B Eng. **195**, 108039 (2020). https://doi.org/10.1016/j.compositesb.2020.108039
2. Rose, J.L.: Ultrasonic guided waves in solid media (2014)
3. Karmazin, A.: Time-efficient simulation of surface-excited guided lamb wave propagation in composites (2012)
4. Cai, J., Yuan, S., Qing, X.P., Chang, F.K., Shi, L., Qiu, L.: Linearly dispersive signal construction of Lamb waves with measured relative wavenumber curves. Sensors Actuators A Phys. **221**, 41–52 (2015). https://doi.org/10.1016/j.sna.2014.10.037
5. Pahlavan, L.: Wave propagation in thin-walled composite structures: application to structural health monitoring (2012)
6. Falcetelli, F., Romero, M.B., Pant, S., Troiani, E., Martinez, M.: Modelling of pencil-lead break acoustic emission sources using the time reversal technique. In: Proceedings of the 9th European Workshop on Structural Health Monitoring, Manchester, pp. 10–13 (2018)
7. Falcetelli, F., Venturini, N., Romero, M.B., Martinez, M.J., Pant, S., Troiani, E.: Broadband signal reconstruction for SHM: an experimental and numerical time reversal methodology. J. Intell. Mater. Syst. Struct. **32**, 1043–1058 (2021). https://doi.org/10.1177/1045389X20972474
8. Park, H.W., Sohn, H., Law, K.H., Farrar, C.R.: Time reversal active sensing for health monitoring of a composite plate. J. Sound Vib. **302**, 50–66 (2007). https://doi.org/10.1016/j.jsv.2006.10.044
9. Xu, B., Yu, L., Giurgiutiu, V.: Lamb wave dispersion compensation in piezoelectric wafer active sensor phased-array applications. Heal. Monit. Struct. Biol. Syst. **7295**, 729516 (2009). https://doi.org/10.1117/12.816085
10. Pahlavan, L., Blacquière, G.: Fatigue crack sizing in steel bridge decks using ultrasonic guided waves. NDT E Int. **77**, 49–62 (2016). https://doi.org/10.1016/j.ndteint.2015.09.006
11. Wilcox, P.D.: A rapid signal processing technique to remove the effect of dispersion from guided wave signals. IEEE Trans. Ultrason. Ferroelectr. Freq. Control. **50**, 419–427 (2003). https://doi.org/10.1109/TUFFC.2003.1197965
12. Hall, J.S., Michaels, J.E.: Adaptive dispersion compensation for guided wave imaging. AIP Conf. Proc. **1430**, 623–630 (2012). https://doi.org/10.1063/1.4716285
13. Qiu, J., Li, F., Abbas, S., Zhu, Y.: A baseline-free damage detection approach based on distance compensation of guided waves. J. Low Freq. Noise Vib. Act. Control. **38**, 1132–1148 (2019). https://doi.org/10.1177/1461348418813699
14. Feng, K., Li, Z.: Damage imaging in composite laminates using phase reversal method. AIP Conf. Proc. **2102**, 1–8 (2019). https://doi.org/10.1063/1.5099751
15. Wang, L., Yuan, F.G.: Group velocity and characteristic wave curves of Lamb waves in composites: modeling and experiments. Compos. Sci. Technol. **67**, 1370–1384 (2007). https://doi.org/10.1016/j.compscitech.2006.09.023
16. Palacz, M.: Spectral methods for modelling of wave propagation in structures in terms of damage detection-a review. Appl. Sci. **8**(7), 1124 (2018). https://doi.org/10.3390/app8071124

17. Kim, Y., Ha, S., Chang, F.K.: Time-domain spectral element method for built-in piezoelectric-actuator- induced lamb wave propagation analysis. AIAA J. **46**, 591–600 (2008). https://doi.org/10.2514/1.27046

18. Zaal, A.: Feasibility evaluation of a nondestructive estimation of material properties of FRC structures using ultrasonic guided waves (2021)